# X-ray Diffraction Study of the Correlation between Electrostatic Potential and K-Absorption Edge Energy in a Bis($\mu$-oxo) Mn(III)−Mn(IV) Dimer

**Anette Frost Jensen,*,† Zhengwei Su,‡ Niels K. Hansen,§ and Finn Krebs Larsen†**

Department of Chemistry, Aarhus University, DK-8000 Aarhus C, Denmark, Department of Chemistry, State University of New York at Buffalo, Natural Sciences and Mathematics Complex, Buffalo, New York 14260-3000, and Laboratoire de Minéralogie, Cristallographie et Physique Infrarouge, UA CNRS 809, Université de Nancy I, BP 239, F-54506 Vandoeuvre les Nancy CEDEX, France

*Received October 20, 1994*[⊗]

The mixed-valence compound bis($\mu$-oxo)tetrakis(2,2′-bipyridine)dimanganese(III,IV) is a small molecule model compound for the oxygen-evolving center, an enzyme which converts water into dioxygen in photosystem II in the photosynthesis of green plants and algae. Crystallographic data: $M_r$ = 1077.47 g/mol, monoclinic, $P2_1/c$, $Z$ = 4, $a$ = 13.584(2) Å, $b$ = 14.058(4) Å, $c$ = 23.622(5) Å, $\beta$ = 105.25(2)°, $V$ = 4352(4) Å$^3$ at $T$ = 9 K. A quantitative estimate for the valence contrast, i.e., the difference in electrostatic potential of the two Mn atoms in this compound, has been established by two different experimental methods which both involve single-crystal X-ray diffraction. A resonant synchrotron X-ray diffraction experiment examining the Bragg scattering for energies of the incoming beam close to the Mn absorption edge at 6539 keV (~1.9 Å wavelength) shows a 3.7 eV difference in ionization energies of the first K-shell electron for Mn(IV) and Mn(III), respectively. The Mn(IV) edge has the higher energy. Low-temperature (9 K) X-ray diffraction data allowed a multipolar refinement of the electron density distribution. The most remarkable feature of the deformation density maps is a large accumulation of density at the $\mu$-oxygen atoms inside the planar 4-membered Mn(III)−O−Mn(IV)−O ring. From the electron density, the electrostatic potential at each of the manganese nuclei has been calculated, first using a direct space summation and, second, a Fourier summation combined with an atomic cluster calculation. When corrected for the energy term, which originates from relaxation of the remaining electrons upon removal of one electron, the two calculations give estimates of valence shifts of the ionization energy of 4.0 and 2.9 eV, respectively. These values closely bracket the value of 3.7 eV obtained in the resonant synchrotron X-ray diffraction experiment, and they are in good accordance with the result, 3.2 eV, of an all-electron ab-initio model calculation. It is to the authors' knowledge the first attempt to compare values of shifts in core-ionization energies as found from the two different types of diffraction experiments.

## Introduction

The purpose of the present study is to examine experimentally if a correlation between valency as defined by X-ray absorption edge position and the electrostatic potential derived from the charge density distribution exists.

We present an experimental charge density determination from 9 K X-ray diffraction data of the tetrafluoroborate salt of the mixed-valence complex cation bis($\mu$-oxo)tetrakis(2,2′-bipyridine)dimanganese(III,IV) **1** and a calculation of the valence shift in the electrostatic potential of the two manganese nuclei. The valence shift of the K-absorption edge of the crystallographically distinct Mn(III) and Mn(IV) atoms has previously been determined to be 3.7 eV by means of valence-selective diffraction at the K-absorption edge using an X-ray synchrotron source.[1]

It is the first time this type of comparison has been attempted, and this paper thus represents a proof of principle. This study is the first in a series of compounds for which the approach will be applied.

Compound **1** is an organometallic mixed-valence compound. Since the reviews in 1967 by Robin and Day[2a] and by Allen and Hush,[2b] there has been a considerable research interest in these compounds. The concept of mixed-valence compounds is very important in biology and bioinorganic chemistry because enzyme chemistry often involves metal ions in different valences. Robin and Day[2a] divided mixed-valence compounds in three classes according to the extent of delocalization of electrons between the, at minimum two, metal centers. Class I is completely valence trapped, i.e., there is no interaction between the centers. Class III is completely delocalized, i.e., the metal centers are indistinguishable because of fast electron transfer between the centers. In between those two groups is class II, where some interaction is present, but the metal centers are still distinguishable. Spectroscopic evidence indicates that the complex **1** in solution is a class II compound.

Complex **1** has been investigated in great detail because it is a model compound for the oxygen-evolving complex in photosystem II in the photosynthesis in green plants, where water is converted into dioxygen.[3a−d] This center is known to contain 4 manganese atoms which are sequentially oxidized in a four-step cycle, the so-called oxygen clock. There are five states of

* Present address: European Synchrotron Radiation Facility, Experimental Division, B.P. 220, F-38043 Grenoble Cedex, France. Author to whom correspondence should be addressed.

† Aarhus University.

‡ State University of New York at Buffalo.

§ Université de Nancy.

⊗ Abstract published in *Advance ACS Abstracts,* June 1, 1995.

(1) Gao, Y.; Jensen, A. F.; Pressprich, M. R.; Coppens, P.; Marquez, A.; Dupuis, M. *J. Am. Chem. Soc.* **1992**, *114*, 9214.

(2) (a) Robin, M. B.; Day, P. *Adv. Inorg. Chem. Radiochem.* **1967**, *10*, 247. (b) Allen, G. C.; Hush, N. S. *Prog. Inorg. Chem.* **1967**, *8*, 357.

(3) (a) Dismukes, G. C. *Photochem. Photobiol.* **1986**, *43*, 99. (b) Pecoraro, V. L. *Photochem. Photobiol.* **1988**, *48*, 249. (c) Brudvig, G. W.; Crabtree, R. H. *Prog. Inorg. Chem.* **1989**, *37*, 99. (d) Thorp, H. H.; Brudvig, G. W. *New J. Chem.* **1991**, *15*, 479.

0020-1669/95/1334-4244$09.00/0 

the oxygen-evolving complex, called $S_0$, $S_1$, $S_2$, $S_3$, and $S_4$. $S_0$ and $S_1$ are in principle infinitely stable, while $S_2$ and $S_3$ have lifetimes ranging between several seconds and minutes, and $S_4$ is extremely unstable (microseconds). Between each state absorption of a photon leads to release of one electron. Oxidation of manganese is believed to occur in most cycles, though it is uncertain as to whether the transition $S_2$ to $S_3$ involves oxidation of Mn. Most effort of small molecule modeling has been concentrated on the states $S_0$, $S_1$, and $S_2$. This has led to a variety of mixed-valence di-, tri-, and tetranuclear manganese complexes, the manganese nuclei being bridged by one, two, or three $\mu$-oxo, $\mu$-hydroxo, or $\mu$-carboxylato bridges, since from X-ray absorption spectroscopy (EXAFS) studies on photosystem II,[4a-e] it is evident that a coordination sphere at 1.8−1.9 Å exists, which fits a Mn(III)−O distance, and other metal (Mn) atoms are present at 2.7 Å and at 3.3 Å. A distance of 2.7 Å is obtained in a bis($\mu$-oxo)-bridged Mn(III)−Mn(IV) core, while 3.3 Å can be obtained by bis($\mu$-oxo)-$\mu$-carboxylato bridging of Mn(III)−Mn(III). Although many features of the oxygen-evolving complex and the model compounds have been revealed and a few reaction mechanisms have been suggested (Brudvig and Crabtree,[5a] Vincent and Christou[5b]), the structure of the oxygen-evolving complex itself remains unknown. Recent theoretical work by Proserpio, Hoffmann, and Dismukes[6] showed all of the present models considered to have very large activation energies for the structural change needed in the proposed mechanism for $O_2$ evolution. In particular, they tested the bridging of a pair of $\mu$-oxygen atoms to form and release dioxygen and calculated an activation energy of about 5 eV for a $(Mn(IV)-\mu-O)_2(OH_2)_8$ unit.

We have undertaken the first electron density determination of a model compound for the oxygen-evolving complex. Compound **1** was first synthesized as the persulfate and subsequently as the perchlorate salt by Nyholm and Turco.[7a] The latter compound crystallizes in space group $P2_1/c$ with 70 non-hydrogen atoms in the asymmetric unit, as determined by Plaksin et al.[7b] Their study revealed very different geometries at the two Mn nuclei, allowing for a clear allocation of valence states as Mn(III) and Mn(IV), both in octahedral coordination, the Mn(III) octahedron being Jahn−Teller distorted.

Spectroscopic, magnetic, and electrochemical measurements were published by Cooper et al.[8a,b] EPR spectroscopic measurements (in $10^{-3}$ M $CH_3CN$ at 18 K) give an anisotropically broadened multiline (16 lines) signal, centered at $g = 2.0$ and with hyperfine structure, due to two nonequivalent $^{55}Mn$ ($I = {}^5/_2$) nuclei. This is interpreted to correspond to the localization of the unpaired electron on one of the nuclei or, alternatively, to a very slow electron transfer rate ($<10^8$ $s^{-1}$). A similar multiline EPR signal at $g = 2.0$ is observed for the $S_2$ state of the oxygen-evolving complex. It disappears on reduction to the $S_1$ or oxidation to the $S_3$ state.

Magnetic susceptibility measurements indicate an $S = (2,{}^3/_2)$ spin system, with antiferromagnetically coupled Mn atoms and a coupling constant of $J = -150(7)$ $cm^{-1}$ per nuclei.[8b] This shows the unpaired $e_g$ electron to be localized on Mn(III). The magnetic moment, corrected for a diamagnetic contribution, per dimer is $\mu = 2.46$ $\mu_B$ (298 K) decreasing to $\mu = 1.74$ $\mu_B$ at 4 K, corresponding to a spin-only value of $S = {}^1/_2$, $\mu = 1.73$ $\mu_B$. This indicates a high-spin Mn(III) ion, since a low-spin complex would be anticipated to have an orbital angular momentum contribution to $\mu$ at low temperature.[8b]

The optical absorption spectrum was measured from a pH = 4.5 solution with bipyridine as the buffer.[8a] The spectrum shows similarities to that of $Mn(III)L_6$ octahedral complexes, L being a ligand with N or O bound to Mn, with bands at 525 and 555 nm, which are ascribed d−d transition bands specific for octahedral symmetry, while a band at 684 nm is due to a ligand (O) to metal charge transfer. There is, however, a broad band in the near-IR region, assumed to peak at 830 nm. This band is observed neither for $Mn(III)L_6$ complexes nor for the bis($\mu$-oxo)dimanganese(IV,IV) tetrakis(1,10-phenanthroline) complex.[8a] It is ascribed to an intervalence transfer, originating by transfer of an electron from Mn(III) to Mn(IV). The occurrence of the 830 nm band classifies the compound into the Robin and Day class II.[2a]

Cyclic voltammetric experiments controlled by potential coulometry performed in acetonitrile show the conversion of the dimanganese(IV,IV) complex to the dimanganese(III,IV) complex to be a one-electron process.[8a] It is facile and reversible, while reduction to the dimanganese(III,III) complex is less facile and irreversible.

These chemical and physical properties are not unique for the present compound but typical for the whole class of bis($\mu$-oxo)-bridged mixed-valence dimanganese(III,IV) compounds.[9a-f] It is noted that a peculiarity of this class of compounds is that they are all poor scatterers at high sin $\theta/\lambda$ values, presumably due to crystallographic disorder of anions or even atoms belonging to the cation complexes themselves. This inherently renders a state-of-the-art electron density determination impossible.

## Experimental Section

**Synthesis.** The synthesis of the tetrafluoroborate salt of **1** was performed as previously described for the perchlorate salt,[8a] except that $NaBF_4$ was substituted for $NaClO_4$. Recrystallization was performed from a 0.05 M bipyridine/bipyridinium buffer at pH = 4.5 (nitric acid) saturated with the dimanganese(III,IV) complex. The solution was heated to 50 °C and filtered while hot and allowed to crystallize over $1{}^1/_2$ days. Small platelike pseudotriangular crystals were obtained.

**X-ray Data.** A crystal was sealed in a capillary tube and mounted on a HUBER four-circle diffractometer. A data set at 292 K was collected with monochromated Ag Kα radiation using $\omega-2\theta$ scans. A total of 3823 unique reflections ($1° < 2\theta < 30°$) was collected, of which 1736 had $I > 3\sigma(I)$, and were used in the structure determination. Information concerning this data collection has been deposited as supporting information in Table S1a. At a later stage, a second crystal

(4) (a) Kirby, J. A.; Robertson, A. S.; Smith, J. P.; Thompson, A. C.; Cooper, S. R.; Klein, M. P. *J. Am. Chem. Soc.* **1981**, *103*, 5529. (b) Yachandra, V. K.; Guiles, R. D.; McDermott, A.; Britt, R. D.; Dexheimer, S. L.; Sauer, K.; Klein, M. P. *Biochim. Biophys. Acta* **1986**, *850*, 324. (c) Yachandra, V. K.; Guiles, R. D.; McDermott, A.; Cole, J. L.; Britt, R. D.; Dexheimer, S. L.; Sauer, K.; Klein, M. P. *Biochemistry* **1987**, *26*, 5974. (d) George, G. N.; Prince, R. C.; Cramer, S. P. *Science* **1989**, *243*, 789. (e) Penner-Hahn, J. E.; Fronko, R. M.; Pecoraro, V. L.; Yocum, C. F.; Betts, S. D.; Bowlby, N. R. *J. Am. Chem. Soc.* **1990**, *112*, 2549.

(5) (a) Brudvig, G. W.; Crabtree, R. H. *Proc. Natl. Acad. Sci., U.S.A.* **1986**, *83*, 4586. (b) Vincent, J. B.; Christou, G. *Inorg. Chim. Acta* **1987**, *136*, L41.

(6) Proserpio, D. M.; Hoffmann, R.; Dismukes, G. C. *J. Am. Chem. Soc.* **1992**, *114*, 4374.

(7) (a) Nyholm, R. S.; Turco, A. *Chem. Ind. (London)* **1960**, 74. (b) Plaksin, P. M.; Stoufer, R. C.; Mathew, M.; Palenik, G. J. *J. Am. Chem. Soc.* **1972**, *94*, 2121.

(8) (a) Cooper, S. R.; Calvin, M. *J. Am. Chem. Soc.* **1977**, *99*, 6623. (b) Cooper, S. R.; Dismukes, G. C.; Klein, M. P.; Calvin, M. *J. Am. Chem. Soc.* **1978**, *100*, 7248.

(9) (a) Stebler, M.; Ludi, A.; Bürgi, H.-B. *Inorg. Chem.* **1986**, *25*, 4743. (b) Hagen, K. S.; Armstrong, W. H.; Hope, H. *Inorg. Chem.* **1988**, *27*, 967. (c) Goodson, P. A.; Glerup, J.; Hodgson, D. J.; Michelsen, K.; Pedersen, E. *Inorg. Chem.* **1990**, *29*, 503. (d) Brewer, K.; Calvin, M.; Lumpkin, R. S.; Otvos, J. W.; Spreer, L. O. *Inorg. Chem.* **1989**, *28*, 4446. (e) Suzuki, M.; Senda, H.; Kobayashi, Y.; Oshio, H.; Uehara, A. *Chem. Lett.* **1988**, 1763−1766. (f) Towle, D. K.; Botsford, C. A.; Hodgson, D. J. *Inorg. Chim. Acta* **1988**, *141*, 167.

**Table 1.** Crystallographic Data for Bis($\mu$-oxo)tetrakis(2,2′-bipyridine)dimanganese(III,IV) Tris(tetrafluoroborate) Trihydrate

| | |
|---|---|
| chemical formula | $(MnO)_2(N_2C_{10}H_8)_4(BF_4)_3(H_2O)_{2.8}$ |
| $a$, Å | 13.584(2) |
| $b$, Å | 14.058(4) |
| $c$, Å | 23.622(5) |
| $\beta$, deg | 105.25(2) |
| $V$, Å$^3$ | 4352(4) |
| $Z = 4$ | |
| formula weight $M_r$, g/mol | 1077.47 |
| space group | $P2_1/c$, No. 14 |
| $T$, K | 9 |
| $\lambda$, Å | 0.7107 |
| $\varrho_{calc}$, g/cm$^3$ | 1.644 |
| $\mu$, cm$^{-1}$ | 7.25 |
| $^a R(F_o)$ | 0.0431 |
| $^a R_w(F_o)$ | 0.0330 |

$^a$ Definition of $R$ factors: $R(F_o) = \Sigma(||F_o|/k - |F_c||)/\Sigma|F_o|$, $R_w(F_o) = (\Sigma w((|F_o|/k) - |F_c|)^2/\Sigma w|F_o|^2)^{1/2}$, $w = 1/\sigma^2(F)$, $\sigma(F^2) = (\sigma_{cts}^2(F_o^2) + (1 + a)F_o^2)^{1/2} - |F_o|$.

in a capillary tube was mounted on a DISPLEX closed-cycle He-cryostat on the same diffractometer, cooled to 9 K, and used for data collection with monochromated Mo K$\alpha$ radiation, $1° < 2\theta < 44°$. Since the intensity of the reflections quickly diminished with increasing $\sin\theta/\lambda$, no data beyond $2\theta = 44°$ were collected, giving $(\sin\theta/\lambda)_{max} = 0.53$ Å$^{-1}$. Unit cell dimensions at 9 K were obtained by least-squares fit using positional angles of the K$\alpha_1$ peaks of 53 reflections in the range $40° < 2\theta < 44°$. For this latter experiment, data were collected in three quadrants, in total 5633 unique reflections, of which 3346 had $I > 3\sigma(I)$. Short-term temperature variations were less than 0.2 K through the scanning period of each reflection measurement. The temperature rose slightly from 8.3 to 10.4 K during the data collection period of 24 days. Crystallographic data are summarized in Table 1; experimental information can be found in Table S1b, submitted as supporting information.

**Data Reduction.** The data were integrated using trapezoidal integration, and peak limits were determined using the minimum $\sigma(I)/I$ method.[10] Corrections for Lorentz and polarization effects were performed and absorption was corrected for, using the Gaussian integration method. Minimum and maximum transmissions were 90% and 96%. The X-ray intensity showed a decay of 4% over the data collection period, and the data were scaled with a first-degree polynomial fitted to the standard reflection intensities. Data were sorted and averaged, yielding an overall internal $R$ value of 3.45%, though for large reflections with $I > 50\sigma(I)$, $R$ was 1.60%. All of the above data reduction was performed using a local program package, partly based on Blessings programs.[11] Further details of data reduction are shown in Table S1b (deposited).

## Structure Solution and Refinement

**Spherical Atom Model.** A spherical atom least-squares refinement with non-hydrogen atoms showed the room temperature structure to be isomorphous with that of the previously studied perchlorate, and the structure refinement was started from a set of coordinates derived from that compound.[7b] No phase transitions were observed in the temperature range 292 to 8 K. For the low-temperature data, hydrogen atoms were located with difference Fourier methods. The least-squares refinement, performed with LINEX84,[12] minimized the function $\Sigma w(|F_o|/k - |F_c|)^2$, $w = 1/\sigma^2(F)$, $\sigma(F^2) = (\sigma_{cts}^2(F_o^2) + (1 + a)F_o^2)^{1/2} - |F_o|$, where $a = 0.03$ is an experimental instability factor. Mn and $\mu$-O atoms were refined with anisotropic thermal parameters while F, water-O, N, C, B, and H were kept isotropic. Two different models were tested. In one model, the positional coordinates of all atoms were allowed to vary, while in the other model a constraint was imposed on the parameters to give identical geometry to the chemical identical entities: a $NC_5H_4$ unit, a $BF_4$ unit, and an $H_2O$ unit. The atom parameters of one unit were refined together with Eulerian angles and translation vectors for all identical units. In the program, the derivatives for all atoms in all molecules are transformed and added to those of the unit refined. The constrained model was finally deemed most reasonable, since the geometry obtained was chemically sound and the number of variables was more than halved. Neutral atom scattering factors were taken from ref 13 for Mn, F, O, N, C, and B. The hydrogen atom scattering factor was that of Stewart *et al.*[14] The final refinement figures of merit are listed in Table 2. A drawing[15] of the complex cation is shown in Figure 1.

**Table 2.** Information about Refinements

| | spherical free atom model | spherical constrained model | aspherical constrained model |
|---|---|---|---|
| $N_{obs}$ | 3345 | 3342 | 3346 |
| $N_{var}$ | 456 | 179 | 239 |
| scale | 0.07886(12) | 0.07856(14) | 0.07870(3) |
| g.o.f. | 1.261 | 1.271 | 1.723 |
| $R(F)$, $R_w(F)$ | 0.0420, 0.0400 | 0.0475, 0.0509 | 0.0431, 0.0330 |
| $R(F^2)$, $R_w(F^2)$ | 0.0600, 0.0800 | 0.0695, 0.1011 | 0.0604, 0.0657 |
| refined on | $F$ | $F$ | $F^2$ |
| $\sin\theta/\lambda$ range | 0.02 to 0.54 | 0.02 to 0.54 | 0.02 to 0.54 |

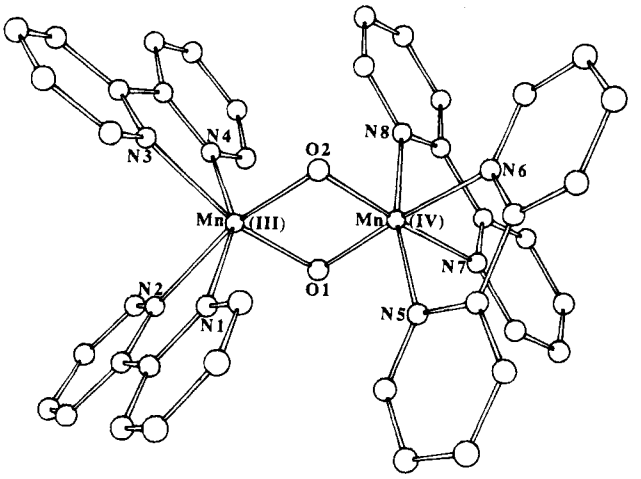


**Figure 1.** ORTEP drawing of the complex cation bis($\mu$-oxo)-dimanganese(III,IV) tetrakis(2,2′-bipyridine) with 50% probablity ellipsoids from 9 K data. Unlabeled atoms are carbon. Hydrogen atoms have been omitted.

**Aspherical Atom Model.** In the aspherical atom refinements with the program MOLLY, the electron density at each atom is described according to Hansen and Coppens[16] by an expansion of atom-centered density functions. For manganese:

$$\varrho_{Mn}(r) = \varrho_{core}(r) + \kappa'^3 P_{4s}\varrho_{4s}(\kappa' r) + \kappa''^3 P_{3d}\varrho_{3d}(\kappa'' r) + \sum_{l=2}^{4} \kappa''^3 \varrho_{3d}(\kappa'' r) \sum_{m=-l}^{l} P_{lm\pm} y_{lm\pm}$$

For the other non-hydrogen atoms:

$$\varrho_{atom}(r) = \varrho_{core}(r) + \kappa'^3 P_{val}\varrho_{val}(\kappa' r) + \sum_{l=1}^{3} \kappa''^3 R_l(\kappa'' r) \sum_{m=-l}^{l} P_{lm\pm} y_{lm\pm}$$

The generalized scattering factors corresponding to $\varrho_{core}$, $\varrho_{val}$, $\varrho_{4s}$, and $\varrho_{3d}$ are spherical core and valence densities. They are computed by

(10) Lehmann, M. S.; Larsen, F. K. *Acta Crystallogr., Sect. A* **1974**, *A30*, 580.
(11) Blessing, R. H. *Crystallogr. Rev.* **1987**, *1*, 3.
(12) LINEX84, S.U.N.Y. at Buffalo, based on Busing, W. R.; Martin, K. O.; Levy, H. A. ORFLS. Report no. ORNL-TM-305; Oak Ridge National Laboratory: Oak Ridge, TN, 1964. Modified by V. Petricek to include rigid body treatment.
(13) *International Tables of X-ray Crystallography*; Kynoch Press: Birmingham, England, 1974; Vol. IV.
(14) Stewart, R. F.; Davidson, E. R.; Simpson, W. T. *J. Chem. Phys.* **1965**, *42*, 3175.
(15) Johnson, C. K. ORTEPII. Report no. ORNL-5138; Oak Ridge National Laboratory: Oak Ridge, TN, 1976.
(16) Hansen, N. K.; Coppens, P. *Acta Crystallogr., Sect. A* **1978**, *A34*, 909.

MOLLY from the atomic wave functions of Clementi and Roetti.[17] For hydrogen, a single Slater-type orbital was used to describe $\varrho_{val}$. $\kappa'$ and $\kappa''$ are refinable expansion/contraction parameters, and $P_{val}$ and $P_{lm\pm}$ are refinable population coefficients of valence density functions, which are described by radial, $R_l$, and spherical harmonic angular, $y_{lm\pm}$, functions. Radial functions of the Slater-type form $R_l(\kappa''r) = Nr^{n(l)} \exp(-\kappa''\zeta r)$ were used for all non-hydrogen atoms except manganese. The coefficients $\zeta$ were selected from ref 18, with $n_l = (2,2,3)$ for $l = (1,2,3)$. The radial functions of the hydrogen atoms are bond-oriented dipoles and are given by $n = 1$ and $\zeta = 3.86$ bohr$^{-1}$. The local coordinate systems for the individual atoms are defined in Figure S1, which is submitted as supporting information.

At room temperature, the tetrafluoroborate ions, the crystal water molecules, and even the bipyridine carbon atoms are found to have large apparent thermal parameters, conforming with the fact that the compound is a poor scatterer. At 9 K, the fluorine atoms have apparent thermal parameters which are up to twice as large as those of the Mn, $\mu$-O, and N atoms, which may indicate some disorder of the tetrafluoroborate groups. Also at 9 K, the high-angle reflections are weak, though stronger than at 292 K, and their intensity diminishes rapidly beyond $2\theta = 40°$. As a consequence, it was essential to reduce the number of variables in the refinement of the low-temperature structure as well, and a constrained geometry model was chosen as previously described, though Mn and $\mu$-O atoms were given isotropic thermal parameters. Populations of all chemically equivalent atoms were constrained to be identical. The bridging oxygens were constrained to have identical population and thermal parameters, since unconstrained refinements led to instabilities. The eight nitrogen atoms in the bipyridine groups were constrained to be pairwise identical according to their distances to Mn atoms found for the pseudo-octahedral coordination. The four groups are $N_{ax}^{III}$ axially (with respect to the Mn(III)−$\mu$-O1−Mn(IV) plane) bonded to Mn(III), $N_{eqv}^{III}$ equatorially bonded to Mn(III), and likewise $N_{eqv}^{IV}$ and $N_{ax}^{IV}$ bonded to Mn(IV). Constraints for Mn multipoles were taken from Holladay, Leung, and Coppens,[19] i.e., only monopole, quadrupole, and hexadecapole parameters ($l = 0$, 2, and 4) were allowed to refine because they are the only multipoles that correspond to products of d-orbitals. Carbon atoms were constrained to $C_s$ symmetry with respect to the pyridine plane, divided into five different chemical groups. Charge parameters of the hydrogen atoms were all kept identical. The monopole population, describing the valence electrons, on the boron atom was constrained to 3.0 electrons, since it correlated heavily with the fluorine atom monopole. Likewise, the water molecules were made identical and neutral and constrained to $C_s$ symmetry. Each chemically different group was given its own expansion−contraction parameter $\kappa'$, though all carbon atoms had the same $\kappa'$. For the manganese, both $\kappa'$s were fixed at 1.0, while the $\kappa''$s were allowed to vary. The occupation of the monopole with radial dependence as the 4s orbital was set to 0.0 electron, since this charge distribution is so diffuse that it will be represented by the functions on neighboring atoms. The refined monopole had a radial dependence corresponding to that of the 3d orbital.

Since high-order reflections are little affected by bonding, atomic parameters are preferably obtained from those. This, however, is not possible in the present study because of the lack of high-order data, and we observed the atomic positions to correlate with the valence density parameters, which are determined mainly by low-order (low $\sin\theta/\lambda$) reflections. The correlation is obvious for the $\mu$-O atoms—the Mn−$\mu$-O distances on average increase 0.03 Å when going from spherical to aspherical refinement and the $\mu$-O to $\mu$-O distance increases by 0.10 Å. These atomic positions are the only ones that are varied independently in the multipole refinement. This correlation of course is a much more serious problem for light atoms (i.e., H, C, N, O), where the core scattering is low compared to the valence scattering. The Mn positions are much more accurately determined, the coordinates differing less than two estimated standard deviations between aspherical and spherical atom refinements. For all models tested, the Mn−Mn distance remained 2.705(1) Å.

Because of the relatively small number of reflections, only positional parameters for Mn and $\mu$-O were allowed to refine in the multipole refinement, while all other atoms were fixed at positions obtained in the spherical, constrained geometry refinement. These constraints were justified *a posteriori* by the lack of significant differences in the residual maps (deposited as supporting information) between different groups of chemically equivalent bipyridine ligands. Residual maps show the difference between the refined multipole charge density and the total charge density and are thus a measure for the quality of the fit of the model. Final refinement figures of merit are listed in Table 2. Atomic coordinates for Mn, $\mu$-O, and N atoms are listed in Table 3, and the remaining atomic coordinates can be obtained as supporting information (Table S2). The most important bonding distances are listed in Table 4. Bonding angles can be obtained as supporting information (Table S3). Monopole populations ($P_{3d}$ for Mn, $P_{val}$ for remaining atoms) are listed in Table 5, a full list of multipole populations for all atoms can be obtained as supporting information Table S4, and d-orbital populations for Mn atoms are listed in Table S5.

**Table 3.** Atomic Coordinates Corresponding to the Aspherical Model[a]

| atom | $x$ | $y$ | $z$ | $U_{iso}$ (Å$^2$) |
|---|---|---|---|---|
| Mn(III) | 0.25061(6) | 0.07454(6) | 0.18134(4) | 0.01046(0) |
| Mn(IV) | 0.24380(6) | 0.01787(6) | 0.28968(4) | 0.01046(0) |
| O1 | 0.3149(14) | −0.0157(14) | 0.2379(8) | 0.0137(0) |
| O2 | 0.1766(15) | 0.1041(13) | 0.2365(8) | 0.0137(0) |
| N1 | 0.1196(0) | −0.0052(0) | 0.1263(0) | 0.0119(0) |
| N2 | 0.3085(0) | 0.0076(0) | 0.1160(0) | 0.0119(0) |
| N3 | 0.2006(0) | 0.2014(0) | 0.1332(0) | 0.0119(0) |
| N4 | 0.3868(0) | 0.1686(0) | 0.2011(0) | 0.0119(0) |
| N5 | 0.1439(0) | −0.0898(0) | 0.2642(0) | 0.0119(0) |
| N6 | 0.1454(0) | 0.0410(0) | 0.3418(0) | 0.0119(0) |
| N7 | 0.3383(0) | −0.0663(0) | 0.3549(0) | 0.0119(0) |
| N8 | 0.3427(0) | 0.1158(0) | 0.3328(0) | 0.0119(0) |

[a] Note that coordinates for Mn and O atoms are from the multipole refinement, while the N atom coordinates are spherical refinement, since they were not refined in the multipole (aspherical) model. $U_{iso}$ for Mn and O were refined in initial stages but later were fixed at present values. Coordinates of remaining atoms have been deposited (Table S2).

**Table 4.** Bonding Distances

| atoms | distance, Å | atoms | distance, Å |
|---|---|---|---|
| Distances at the Mn-$\mu$-O Core | | | |
| Mn(III)−Mn(IV) | 2.705(1) | | |
| O1−O2 | 2.517(4) | | |
| Mn(III)−O1 | 1.881(3) | Mn(IV)−O1 | 1.809(3) |
| Mn(III)−O2 | 1.891(3) | Mn(IV)−O2 | 1.810(3) |
| Mn(III)−N1 | 2.213(4) | Mn(IV)−N5 | 2.017(4) |
| Mn(III)−N2 | 2.127(4) | Mn(IV)−N6 | 2.067(4) |
| Mn(III)−N3 | 2.129(4) | Mn(IV)−N7 | 2.093(4) |
| Mn(III)−N4 | 2.221(4) | Mn(IV)−N8 | 2.004(4) |
| Distances within a Pyridine Unit | | | |
| N1−C12 | 1.354(6) | | |
| C12−C13 | 1.384(6) | | |
| C13−C14 | 1.378(7) | C13−H13 | 0.95(4) |
| C14−C15 | 1.381(7) | C14−H14 | 0.96(5) |
| C15−C16 | 1.372(7) | C15−H15 | 0.95(5) |
| C16−N1 | 1.343(6) | C16−H16 | 0.93(4) |
| Distances Bridging Pyridine Units | | | |
| C12−C22 | 1.480(6) | C52−C62 | 1.477(7) |
| C32−C42 | 1.475(6) | C72−C82 | 1.475(7) |

## Results and Discussion

**Structure.** The bond lengths to the two Mn atoms clearly indicate that they are of different valence. ⟨Mn(IV)−O⟩ = 1.810(3) Å and ⟨Mn(III)−O⟩ = 1.885(4) Å. Furthermore, there is indication of Jahn−Teller distortion of Mn(III), compatible with a $d^4$ high-spin ion in an octahedral field. The bond lengths for Mn(III) to the axial nitrogen atoms are 2.213(4) and 2.221-

(17) Clementi, E.; Roetti, C. *At. Data Nucl. Data Tables* **1974**, *14*, 177.
(18) Murrell, J. N.; Kettle, S. F. A.; Tedder, J. M. *Valence Theory*, 2nd ed.; John Wiley and Sons, Ltd. London 1970; p 32.
(19) Holladay, A.; Leung, P.; Coppens, P. *Acta Crystallogr., Sect. A* **1983**, *A39*, 377.

**Table 5.** Monopole Populations from the Multipole Refinement

| atom | $P_{val}$ in electrons | atom | $P_{val}$ in electrons |
|---|---|---|---|
| Mn(III) | 5.15(12) | C13 | 3.87(11) |
| Mn(IV) | 4.88(14) | C14 | 4.22(12) |
| $\mu$-O | 7.26(8) | C15 | 3.94(11) |
| $N^{III}_{ax}$ | 5.71(16) | C16 | 3.95(13) |
| $N^{III}_{eqv}$ | 5.66(16) | bpy-H | 0.87(8) |
| $N^{IV}_{ax}$ | 5.80(16) | F | 7.02(2) |
| $N^{IV}_{eqv}$ | 5.62(16) | B | 3.00(0) |
| C12 | 3.97(10) | water-O | 6.00(0) |
| | | water-H | 1.00(0) |

(4) Å, and to the equatorial nitrogen atoms, they are 2.127(4) and 2.129(4) Å. For Mn(IV), the equatorial nitrogen bonds of 2.067(4) and 2.093(4) Å are longer than the Mn(IV) bonds to the axial nitrogen atoms of 2.004(4) and 2.017(4) Å. The octahedral coordination polyhedra are significantly distorted, angles ranging from 75.2(1)° to 106.8(1)° for Mn(III) and from 78.8(2)° to 96.8(1)° for Mn(IV) for angles that would be 90° in a perfect octahedron. O2 deviates 0.02 Å from the Mn(III)−O1−Mn(IV) plane, while $N^{III}_{eqv}$ atoms deviate ±0.50 Å and $N^{IV}_{eqv}$ atoms deviate ±0.30 Å from the Mn(III)−O1−Mn(IV) plane. When a sample is cooled, the *a*- and *c*-axes decrease 1.1% and 1.7%, respectively, while the *b*-axis remains essentially unchanged. The $\beta$ angle changes from 103.7° to 105.2°. At room temperature, the $BF_4$ ions undergo large rotational disorder, as is evident from large anisotropic apparent thermal parameters, which accounts for a relatively early fall off of the scattering ability as a function of $\sin\theta/\lambda$. Even at 9 K, the displacement parameters of the fluorine atoms are quite high, indicating residual disorder.

It has been necessary to apply strong constraints in order to obtain a reasonable parameter-to-observable ratio in the refinement of the electron density parameters. However, the relative population parameters, as well as the features in maps of the manganese, $\mu$-oxygen, and nitrogen atoms, appeared very robust to changes in the detailed modeling, and the qualitative features of the maps, such as density in C−C bonds, $H_2O$ groups, and $BF_4$ groups, are all in good agreement with other studies reported in the literature.

**Charges.** The charge of an atom is defined as the atomic number minus the core and monopole populations, $q = Z - P_{core} - P_{val}$.[16] The observed charge of Mn(III) is +1.85(12)e, and that of Mn(IV) is +2.12(14)e. The charge difference of 0.27(18)e is not statistically significant. However, in all the tested refinement models, the difference remained of the same magnitude and sign. The high charges on the $\mu$-oxygen atoms of −1.26(8) electrons are partly a result of the assumed model of diffuse 4s electrons of Mn. Even when the 4s electrons were placed on Mn, the charge of $\mu$-oxygen atoms was −0.8e. As the apparent thermal vibration parameters and the expansion−contraction parameters $\kappa$ correlate strongly, the thermal vibration parameters were fixed at the spherical atom refinement values. The Mn and $\mu$-O atoms were described with isotropic thermal vibration parameters, as were the remaining atoms. The charge of −1.3e on $\mu$-O is comparable to values obtained for oxygen atoms in ionic solids like potassium titanyl phosphate.[20] The charge values of the ligand nitrogen atoms range from −0.62(16)e to −0.80(16)e. The magnitude of charge is comparable to that of N bonded to Co in the tetraphenylporphyrin (TPP) compound CoTPP[21a] (−0.77(9)e with diffuse 4s electrons) though somewhat higher than for those of corresponding FeTPP[21b] compounds (−0.21(17)e, −0.44(3)e). The charges of the C atoms are ranging from −0.22(12) to +0.13(11)e. The charges obtained (slightly positive for all but one carbon atom) agree quite well with those obtained for the pyrrole rings in $FeTPP(THF)_2$.[21b] All hydrogen atoms on the bipyridines were constrained to have the same population. The charge of +0.13(9)e agrees quite well with similar hydrogen atoms on the porphyrines.[21a-c]

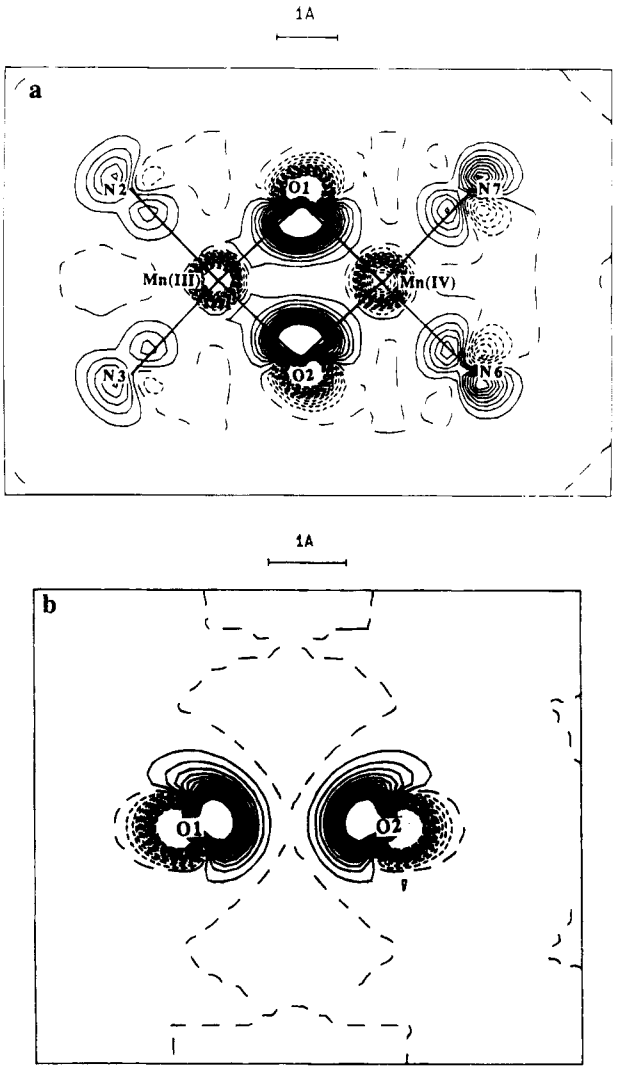


**Figure 2.** (a) Static deformation map in the Mn(III)−O1−Mn(IV) plane. Note that the nitrogen atoms are outside the defined plane. All the following maps are drawn with contours of 0.10 e/Å$^3$ in the interval from −1.5 to 1.5 e/Å$^3$. Negative contours are short dashed, the zero contour has long dashes, and the positive contours are full lines. (b) Static deformation map through O1 and O2 perpendicular to the Mn(III)−O1−Mn(IV) plane. Contours as for a.

**Deformation Densities.** Only static deformation maps are shown; all dynamic deformation density maps have been deposited, as well as some of the residual maps. A static deformation density is a charge density difference between that of the multipole model and the spherical atom model of the molecule with the thermal vibrations deconvoluted.[22]

**The Mn−$\mu$-Oxo Core.** Maps are shown in Figures 2a−b (note that the nitrogen atoms are outside the shown section). The predominant feature in the deformation maps is the large accumulation of density inside the ring at the $\mu$-oxygen atoms

(20) Hansen, N. K.; Protas, J.; Marnier, G. *Acta Crystallogr., Sect. B* **1991**, *B47*, 660.

(21) (a) Stevens, E. D. *J. Am. Chem. Soc.* **1981**, *103*, 5087. (b) Lecomte, C.; Blessing, R. H.; Coppens, P.; Tabard, A. *J. Am. Chem. Soc.* **1986**, *108*, 6942. (c) Li, N.; Coppens, P.; Landrum, J. *Inorg. Chem.* **1988**, *27*, 482.

(22) Coppens, P. *Electron Distributions and the Chemical Bond*; Coppens, P., Hall, M., Eds.; Plenum Press: New York, 1982; pp 61−92.

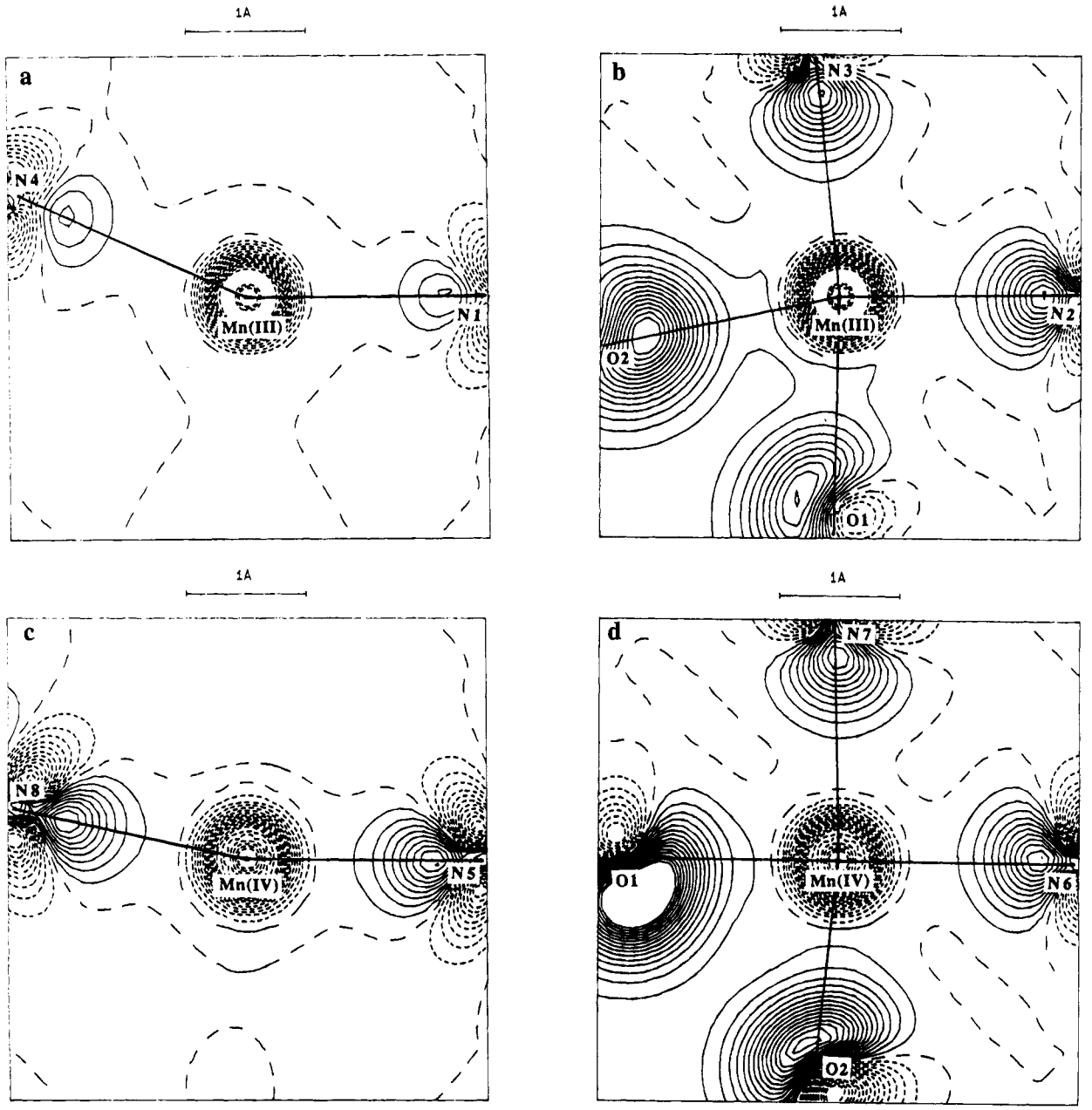


**Figure 3.** (a) Static deformation density map through Mn(III) and N1 and N4 (axial nitrogen atoms). Contours as for Figure 2a. (b) Static deformation density map through Mn(III) and N2 and N3 (equatorial nitrogen atoms). Contours as for Figure 2a. (c) Static deformation density map through Mn(IV) and N5 and N8 (axial nitrogen atoms). Contours as for Figure 2a. (d) Static deformation density map through Mn(IV) and N6 and N7 (equatorial nitrogen atoms). Contours as for Figure 2a.

and the depletion of density on Mn atoms evident from the Mn(III)−O1−Mn(IV) plane section in Figure 2a. The O1−O2 distance is 2.5 Å, and a cross section perpendicular to the Mn−$\mu$−O plane through the $\mu$-O atoms is shown in Figure 2b. No particular aspherical features are observed around the Mn atoms, probably because of the lack of high-order data, which detail the information about the density close to the nucleus. The N2 and N3 ($N^{III}_{eqv}$) atoms have been constrained to have identical populations, and likewise have N6 and N7 ($N^{IV}_{eqv}$) atoms been constrained. The appearance of nitrogen atoms in the static map (Figure 2a) agrees well with chemical intuition, showing one lobe pointing toward the Mn atom and one lobe away from Mn. Lobes of equatorial nitrogen atoms are very similar, and only because N6 and N7 are closer to the shown section in Figure 2a than are N2 and N3 do the lobes of the former set of atoms appear higher.

Figures 3a−d show planes through the manganese and the nitrogen atoms shown in the maps. From these maps, it is possible to compare the bonding of N to Mn. It is evident that the axial nitrogen density lobes (N1 and N4) to Mn(III) are of considerably lower density than the lobes at equatorial nitrogen atoms (N2 and N3) and lower than the density lobes at the nitrogen atoms of Mn(IV). This feature is in good agreement with the observed geometric Jahn−Teller effect, which pushes the axial nitrogen atoms away from Mn(III), so that the donation of density from N to Mn is less for those atoms.

**Bipyridine Units.** A static deformation map of one of the bipyridine units is shown in Figure 4. Maps of remaining bipyridine units have been deposited, Figures S4a−c. They deviate only slightly from the map in Figure 4 at the nitrogen positions. It is evident that density is accumulated in the chemical bonds. The qualitative features observed in one-half bipyridine unit agree well with those in the pyridine unit of $FeTPP(py)_2$,[21c] but the detailed modeling is not quite satisfactory. The density in C−C bonds would be expected from studies of,

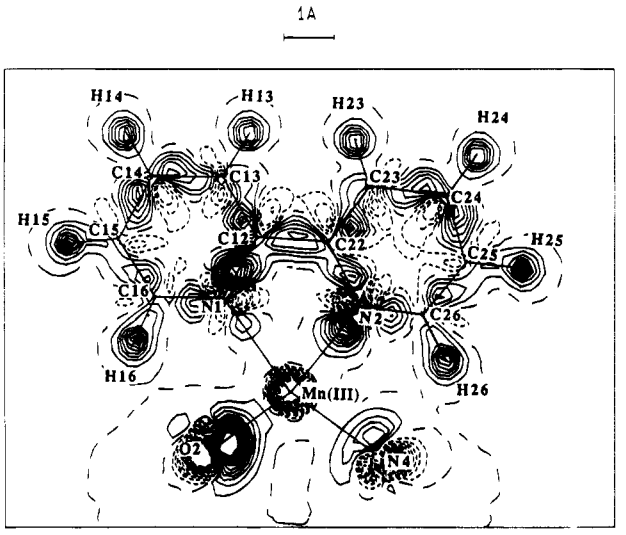


**Figure 4.** Static deformation map showing one bipyridine unit. The map has been constructed so as to show the N1−C12−C16 plane, the N2−C22−C26 plane, and the O2−Mn(III)−N4 plane. The static deformation maps of the remaining three bipyridine units are identical to this one (supporting information). Contours as for Figure 2a.

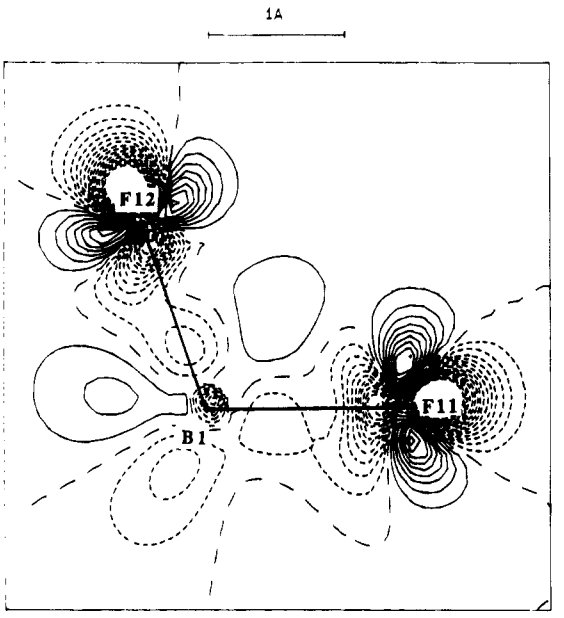


**Figure 5.** Static deformation map in a plane through one boron atom and two fluorine atoms, F11−B1−F12. The five remaining planes (supporting information) have similar features. Contours as for Figure 2a

for instance, porphyrin rings to be symmetrical with respect to the C atoms. For hydrogen atoms, the peak heights have been overestimated, being larger than the peak heights of the C−C bonds. Furthermore, the density at hydrogen atoms should peak between the H and the C atom that it is bonded to, and not at the H atom position. Corresponding deformation maps for porphyrins[21b] show a peak density in a C−H bond of about half the height of a C−C double-bond peak.

**Structurally Related Compounds.** The map showing the density lobes at $\mu$-O corresponds to a model assuming diffuse 4s electrons on manganese. This model inherently increases the peak height in bonds to Mn. However, in all the models we have tested, the peak heights of the $\mu$-O lobes exceed those of the Mn−N bonding peaks. To the best of our knowledge, there is no other electron density study of a binuclear bis($\mu$-oxo) system available for comparison. However, the $(Fe(CO))_2$ core of the bis(dicarbonyl-$\pi$-cyclopentadienyliron)[23] is of some structural similarity. Two Fe atoms are bridged by two carbonyl units in a planar four-membered ring, while two other CO groups are attached to each of the Fe atoms perpendicular to the ring, the crystallographically independent atoms being one Fe, one bridging CO group, and one axial CO group. The dynamic deformation density obtained in that study is much better determined around the Fe nuclei, since data to $\sin\theta/\lambda = 1.15$ Å$^{-1}$ are available. A peak of height 0.30(6) e/Å$^3$ is observed at the carbon atom inside the ring placed symmetrically between the two Fe atoms and the zero contours of the peak meeting the symmetry-related peak of the other carbon atom at the inversion center, reminiscent of the situation in the bis($\mu$-oxo)-dimanganese core. The peak in the C−O bond is of height 0.70(6) e/Å$^3$. The deformation density of Fe in this plane shows four lobes, one of which points into the ring in approximately 4-fold symmetry, the height of the lobe being 0.50(14) e/Å$^3$.

Another electron density study of relevance is that of $Co_2(CO)_8$.[24] The Co atom is pyramidally five-coordinated and linked through two CO units to a symmetry-related unit. The four-membered $(Co(CO))_2$ core is nonplanar. In a dynamic deformation density map in the Co−C(O)−Co half-plane, a lobe of density 0.3(1) e/Å$^3$ is observed at the bridging C atom inside the ring. Because of crystallographic symmetry, it is symmetric with respect to the two bonds to metal atoms. The peak height of the C−O bond is 0.5(1) e/Å$^3$.

Thus, features corresponding to the lobe at $\mu$-O in the ring of the bis($\mu$-oxo)dimanganese core have been observed in other compounds containing two first-row transition metal atoms bridged by light atoms in a four-membered ring, even though the maximum peak heights in our study seem overestimated.

**Tetrafluoroborate Units.** The $BF_4$ units are constrained to all be identical with respect to geometry and populations. The static deformation map of one plane through one boron and two fluorine atoms is shown in Figure 5, while the maps of the remaining five independent planes have been deposited as Figures S5a−e. The maps show absence of density in the B−F bond, but positive lobes on the F atoms in the directions perpendicular to the bond. This density lobe is ring shaped, with a considerable variation in thickness, which could be due to hydrogen bonding of the F atoms. There are negative lobes on F, a small one pointing toward B and a much larger one pointing away from B. This lack of density in the B−F bond agrees quite well with other experimental studies by Hirshfeld *et al.*[25] There is also excellent agreement with a theoretical study by Hall *et al.*[26] on difluorine, which shows no density in the F−F bond but lobes perpendicular to it. Results of the multipole description of the $H_2O$ groups were deemed chemically reasonable from inspection of density in bonds. The static deformation density maps have been deposited as supporting information, Figures S6a−b.

**Resonant Scattering Experiment.** The inelastic scattering of an X-ray photon on a core electron in an atomic orbital leads to excitation of that electron to higher bound or unbound states and thus a loss of elastic scattering intensity. The photon energy at which the inner-shell electron is ionized defines the X-ray absorption edge. By means of X-ray synchrotron radiation, the incoming photon energy can be tuned to a given absorption edge (K shell, $L_I$-, $L_{II}$-, or $L_{III}$-shell electrons ionized) of a given

(23) Mitschler, A.; Rees, B.; Lehmann, M. S. *J. Am. Chem. Soc.* **1978**, *100*, 3390.
(24) Leung, P. C.; Coppens, P. *Acta Crystallogr., Sect. B* **1983**, *B39*, 535.
(25) Hirshfeld, F. L. *Acta Crystallogr., Sect. B* **1984**, *B40*, 613.
(26) Kunze, K. L.; Hall, M. B. *J. Am. Chem. Soc.* **1986**, *108*, 5122.

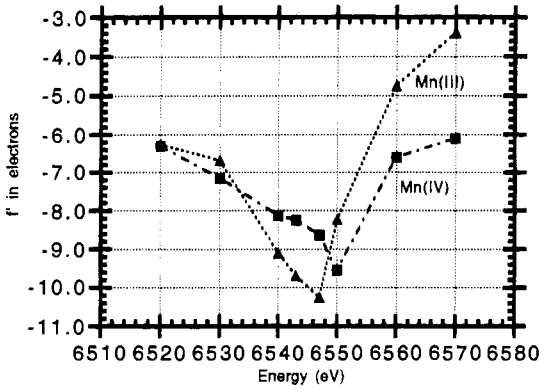


**Figure 6.** Curves showing the real part of the anomalous scattering factor $f'$ versus photon energy for results from the experiment described in ref 1. Data points are triangles for Mn(III) and squares for Mn(IV). The curve is drawn through data points, not fitted.

element. The X-ray form factor ($f = f_o + f'' + if''$) describing the scattering of an element varies as a function of photon energy due to the terms $f'$ and $f''$. The variation is most pronounced at the absorption edge, where the atom is in resonance. In a Bragg diffraction experiment on a crystalline compound, the reflection intensities will be at an extremum at the absorption edge. Provided the crystal structure is known, the anomalous fraction of the form factor ($f'$ and $f''$) can be determined from sets of structure factors measured at different wavelengths.

In a single-crystal X-ray diffraction experiment on compound **1**, a series of 25 Bragg reflections at 8 different photon energies bracketing the manganese K-absorption edge at 6539 eV were measured from 6510 to 6580 eV.[1] The reflections were selected so as to have more than 50% scattering contribution from the Mn(III) and Mn(IV) atoms. By least-squares refinement, $f'(E)$ for Mn(III) and Mn(IV) was determined for the various data sets, and the curves shown in Figure 6 were obtained.[1] That the curves in Figure 6 are broader than the natural line width of the K level which is 1.16 eV for Mn is due to the limited energy resolution of the optics and the beam divergence in the scattering plane at the synchrotron beamline used for the experiment (FWHM was estimated to be 3 eV at 6539 eV). The $f'(E)$ value is at minimum at the absorption edge and the curves, showing the minimum of the Mn(IV) curve at higher energy than that for Mn(III), thus illustrating that the ionization of a K-shell electron requires higher energy for a more positively charged ion. The difference was estimated to be about 3.7(1.0) eV. This experimental finding is in good agreement with an all-electron ab-initio calculation on the $(NH_3)_4Mn^{III}(\mu\text{-}O)_2Mn^{IV}(NH_3)_4$ entity, where the calculated shift was 3.2 eV.[1] The calculation also yielded a charge difference of 0.22e between Mn(III) and Mn(IV) from a Mulliken charge calculation. This difference agrees well with the 0.27(18)e determined from the difference of the monopole populations in our electron density study.

**Calculation of the Electrostatic Potential.** The shift in ionization energy $\Delta I$ for a core electron is related to the shift of the electrostatic potential, $\Delta V$, at the site of the core electron, by[27]

$$\Delta I = \Delta V - \Delta R \qquad (1)$$

$R$ is the energy change of the system due to rearrangement of the remaining electrons occurring upon removal of one core electron (the relaxation effect). This term, $\Delta R$, is often considered negligible in calculations of the ionization energy,

(27) Saethre, L. J.; Siggel, M. R. F.; Thomas, T. D. *J. Am. Chem. Soc.* **1991**, *113*, 5224.

**Table 6.** Estimates of the Chemical Shifts of the K-Shell Ionization Energy and Electrostatic Potential

| | ionization energy shift (eV) | potential shift (eV) |
|---|---|---|
| resonant scattering experiment | 3.7 − 4.0 (1.0) | |
| calculations from e.d. distribution | | |
| method I (Su and Coppens) | 4.0 (2.0) | 3.6 (2.0) |
| method II (Hansen) | 2.9 (0.2)[a] | 2.5 |

[a] Estimated standard deviation must be larger than given, since its contribution from the potential calculation has not been included.

but it can be estimated as follows:[28,29]

$$\Delta R = -1.5\ \Delta q = -0.4(3)\ \text{eV},$$
$$\Delta q = q(\text{Mn(IV)}) - q(\text{Mn(III)}) = 0.27(16)\text{e}$$

Since the electrons contribute a negative value to the total potential and Mn(IV) has formally one electron less than Mn(III), we expect $\Delta V = V(\text{Mn(IV)}) - V(\text{Mn(III)}) > 0$.

The electrostatic potential at the point with position vector $\mathbf{R}_p$ may be written[30]

$$V(\mathbf{R}_p) = \int \varrho_t(\mathbf{r})/|\mathbf{R}_p - \mathbf{r}|\ \mathrm{d}\mathbf{r} = \sum_{i \neq p} Z_i/|\mathbf{R}_p - \mathbf{R}_i| - \sum_i \int \varrho_{e,i}(\mathbf{r} - \mathbf{R}_i)/|\mathbf{r} - \mathbf{R}_p|\ \mathrm{d}(\mathbf{r} - \mathbf{R}_i) \qquad (2)$$

$\varrho_t$ is the total *static* charge density, subsequently split into two terms, where the first term is due to the charges of the nuclei and the second due to the electron densities at each atom, $i$, and $\mathbf{R}_i$ is the direction vector for the nucleus of atom $i$. The sum is over all atoms in the crystal unit cell.

Su and Coppens[30] adopt a direct space approach to evaluate the integral in eq 2 to determine the electrostatic potential at any point in the crystal. The potential at an atomic nucleus is divided into two contributions: the *central* contribution due to the monopole (spherical) density of the atom itself (monopole because only the spherical density at the atom contributes to the potential at the nucleus) and the *peripheral* contributions, which are contributions from all other atoms (the lattice). The two electrostatic potential contributions are expressed in terms of the positions and multipole populations of the atoms obtained in the least-squares refinement.

The electrostatic potential difference between the Mn(IV) and the Mn(III) have been calculated with the program package MOLPROP93[30] using this formalism. The difference obtained can be seen in Table 6.

Hansen[31] adopts another procedure, which is a combination of a Fourier summation technique and an atomic cluster calculation, for calculating the electrostatic potential, similar to the approach described by Stewart.[32]

The expression for the charge density is rewritten

$$\varrho_{\text{multipole}}(\mathbf{R}_p) = \sum_i \varrho^i{}_{\text{atom}}(\mathbf{R}_p - \mathbf{R}_i) + \Delta\varrho(\mathbf{R}_p) \qquad (3)$$

where $\varrho_{\text{multipole}}$ is the total static charge density ($\varrho_t$ in eq 2) as described by the multipole model. The right-hand side of this equation represents a decomposition of the total density into atomic-like contributions and a deformation density which corrects for deficiencies of the atomic description. The nuclear

(28) Gelius, U. *Phys. Scr.* **1974**, *9*, 133.
(29) Snyder, L. C. *J. Chem. Phys.* **1971**, *55*, 95.
(30) Su, Z.; Coppens, P. *Acta Crystallogr., Sect. A* **1992**, *A48*, 188.
(31) Hansen, N. K. *Z. Naturforsch., Sect. A* **1993**, *48A*, 81.
(32) Stewart, R. F. *God. Jugosl. Kristalogr.* **1982**, *17*, 1.

contribution to the charge density is included into the atomic functions which are of spherical symmetry, and it integrates to zero charge. The consequence is that the potential contribution from each atom is short range in nature. The potential contribution from the deformation density is expressed as a Fourier sum

$$V[\Delta\varrho](\mathbf{R}_p) = \frac{1}{\pi V_{\text{cell}}} \sum_{\mathbf{H}\neq\mathbf{0}} \frac{\Delta F(\mathbf{H})}{\mathbf{H}^2} \exp(-2\pi i \boldsymbol{HR}_{i,p}) \quad (4)$$

The difference in structure factors is defined by

$$\Delta F(\mathbf{H}) = F_{\text{multipole}}(\mathbf{H}) - F_{\text{atoms}}(\mathbf{H}) \quad (5)$$

where $F_{\text{multipole}}$ and $F_{\text{atoms}}$ are the Fourier transforms of $\varrho_{\text{multipole}}$ and the atomic term in eq 3, respectively. Summarizing, the electrostatic potential is written

$$V = \sum_i V_{\text{atom}}{}^i + V[\Delta\varrho] \quad (6)$$

Comments on the practical aspects of the computation is given in the Appendix, and the potential difference obtained is listed in Table 6.

## Conclusion

The experimental electron density distribution of the mixed-valence compound bis($\mu$-oxo)tetrakis(2,2′-bipyridine)dimanganese(III,IV) has been determined, as the first of a model compound for the oxygen-evolving center, using a multipolar refinement against observed structure factors derived from X-ray diffraction data measured at 9 K. The most striking feature of the density distribution is a surplus of electron density at the two oxygen atoms inside the four-membered ring.

On the basis of the obtained parameters, the chemical shift between Mn(III) and Mn(IV) in electrostatic potential has been derived by applying two different approaches. The results have been used to calculate the corresponding shifts in ionization energies of the K-shell electron.

The results of the two calculations, 4.0 and 2.9 eV, for the shift in ionization energy agree very well with the result of a resonant scattering experiment measuring the difference in depression of the anomalous scattering form factor $f'$ versus energy yielding a shift of 3.7 eV for a valence shift of formally one electron.

An experimental relation between core electron ionization energy as defined by X-ray absorption edge position and the electrostatic potential at the nucleus derived from the electron density distribution has thus been established. The results, however, are hampered by relatively large standard deviations due to the low resolution of the diffraction data. A quantitative comparison will be attempted in a future study on a compound which diffracts well to high sin $\theta/\lambda$ values.

## Appendix. Calculation of the Electrostatic Potential following Hansen's Method[31]

The electrostatic potential at the nucleus is written

$$V = \sum_i V_{\text{atom}}{}^i + V[\Delta\varrho] \quad (6)$$

where $V^i_{\text{atom}}$ is the term due to a spherical density distribution of an atom calculated from atomic wave functions and $V[\Delta\varrho]$ is the deformation term due to chemical bonding, obtained from a truncated Fourier expansion. Regarding this expression, we want to stress that the partitioning of the density can be done rather freely. This is advantageous from a computational point of view, since we may choose the atomic-like densities such as to give a rapid convergence of the Fourier sum. This may be exemplified by considering two different calculations of the potential. In the first one, we used the charge densities of free atoms[17] for the first terms of the right-hand side of eqs 3 and 6. We found a very poor convergence of $V[\Delta\varrho]$; *i.e.*, different cutoff values in the Fourier synthesis corresponding to maximum values of sin $\theta/\lambda$ between 1.0 and 1.2 Å$^{-1}$ gave oscillations of about 0.5 eV, and one may remark that the number of Fourier coefficients is around 80 000 for the compound studied.

It is recalled that the radial functions used in the multipole model are of the same general shape as for the free atoms, but their radial extent has been modified by the contraction/expansion parameter $\kappa''$ which, for the manganese ions, deviates significantly from 1.00 for the 3d electrons (0.91(2) and 0.94(2), respectively). This gives pronounced oscillations in the deformation density close to the Mn nuclei and, as such, causes the poor convergence of the electrostatic potential at the nucleus. The convergence is considerably improved if we apply the same $\kappa$ values to the atomic density functions as obtained in the multipole model. This is seen from a second calculation which we carried out using this approach; now, the Fourier sum gives practically identical results for all cutoffs corresponding to sin $\theta/\lambda$ above 0.7 Å$^{-1}$.

Concerning the convergence of the first terms in eq 6, there are no problems; by this we mean that we only need to take into account the first coordination shell of the manganese ions. Including all the atoms in a cluster of radius 6 Å centered at the midpoint of the two nuclei only gives an extra contribution of ca. 0.01 eV to the potential.

**Acknowledgment.** We are grateful to professor Philip Coppens, State University of New York at Buffalo, NY, for suggesting the comparison between the resonant scattering chemical shift and the electrostatic potential chemical shift. We are indebted to Dr. Mark R. Pressprich, State University of New York at Buffalo, for performing the synthesis of the crystals. We appreciate valuable discussions with Professor Coppens, Dr. Pressprich, and Mrs. Lanying Wu, also at State University of New York at Buffalo, NY. We would like to thank professor Gus Palenik, University of Florida at Gainesville, FL, for giving us a set of coordinates for the perchlorate salt of **1**. We thank the CNI-MAT (Nancy) for the availability of computing resources necessary for carrying out electrostatic potential calculations by Hansen's method. A student stipend to A.F.J. from the Danish Natural Science Research Council and a post-doctoral fellowship from the Carlsberg Foundation to pursue this work are gratefully acknowledged. We are also indebted to the Carlsberg Foundation for the low-temperature diffractometer in Aarhus.

**Supporting Information Available:** Table of experimental information at room temperature (Table S1a) and at low temperature (Table S1b), listing of atomic coordinates at 9 K (Table S2), listing of bonding angles (Table S3), listing of multipole populations for all individually refined atoms (Table S4), and listing of d-orbital populations (Table S5). Definition of atomic coordinate systems in the multipole refinement (Figure S1), dynamic deformation (Figures S2a–b) and residual (Figure S3) density maps of the Mn-$\mu$–O–Mn-$\mu$–O core, and static deformation density maps of bipyridine units (Figures S4a–c), tetrafluoroborate units (Figures S5a–e), and water molecules (Figures S6a,b) (27 pages). Ordering information is given on any current masthead page.

IC941210D